Optimization and Response Surface Modelling of Activated Carbon Production from Mahogany Fruit Husk for Removal of Chromium (VI) from Aqueous Solution

Bryan John A. Magoling, and Angelica A. Macalalad *

The use of activated carbon (AC) from lignocellulosic wastes has gained a lot of research interest because of its great economic and environmental value. In this work, AC was prepared from mahogany fruit husk (MFH) *via* chemical activation with phosphoric acid and heat treatment. The relationships among the activation parameters H_3PO_4%, heating temperature, and holding time, and their effect on chromium (VI) removal, were investigated using the response surface method (RSM), following a central composite design (CCD). The optimized activation conditions resulted in a 92.3% Cr^{6+} removal efficiency for a 50 mg/L Cr^{6+} aqueous solution. The surface properties of the optimized MFHAC were investigated using scanning electron microscopy (SEM), energy-dispersive X-ray spectroscopy (EDS), Fourier-transform infrared (FTIR) spectroscopy, and nitrogen adsorption/desorption studies. The MFHAC prepared under the optimized conditions had a high surface area (S_{BET}) of 1130 m^2/g, with a well-developed porous structure. The equilibrium data of Cr^{6+} adsorption onto the MFHAC was best fit by the Langmuir isotherm model, while the adsorption kinetic data followed the pseudo-second order kinetic model. Hence, MFHAC proved to be an efficient technology for removing Cr^{6+} from simulated wastewater.

Keywords: Activated carbon; Chromium (VI); Mahogany fruit husk; Response surface method

*Contact information: Department of Chemistry, College of Arts and Sciences, Batangas State University, Rizal Avenue, Batangas City, Philippines; *Corresponding author: aamacalalad@batstate-u.edu.ph*

INTRODUCTION

Industrialization remains one of the most prevalent sources of pollutants in the natural environment. Of these pollutants, heavy metals are considered to be the most toxic because of their inability to be immediately degraded in nature (Al-Othman *et al.* 2011) and their detrimental effect on many living organisms, including humans. Most industrial wastewaters released into the environment consist of undesirable amounts of arsenic, cadmium, chromium, lead, mercury, and nickel. Among these heavy metals, chromium imposes a greater threat to human health because of its solubility in water, which leads to possible contamination of surface and groundwater (Acharya *et al.* 2009). Chromium occurs in the environment in trivalent and hexavalent oxidation states. Chromium (III) is an essential trace element in humans that assists in carbohydrate and fat metabolism, and in maintaining blood glucose levels through regulation of insulin in the body (Setshedi *et al.* 2013), while chromium (VI) (Cr^{6+}) is a known carcinogen and mutagen (Brauer and Wetterhahn 1991). Chromium (VI) also causes dermatitis, ulcers, hemorrhages, pulmonary congestion, and liver damage (Gładysz-Płaska *et al.* 2012; Kushwaha *et al.* 2012).

Process industries that typically discharge chromium (VI) ions in their effluents include leather tanning, electroplating, textile and dye manufacturing, metal plating, and battery production (Jayakumar *et al.* 2014). Thus, there is a great need for the efficient removal of Cr^{6+} from wastewater before it is discharged into the environment. The maximum allowable limit of Cr^{6+} in surface water set by the U.S. Environmental Protection Agency is 0.05 mg/L (Baral and Engelken 2002), and the maximum permissible level of Cr^{6+} in drinking water is 0.05 mg/L (World Health Organization 2011).

Several treatment processes have been applied for the removal of chromium (VI) from wastewaters, such as precipitation, ultrafiltration, ion exchange, and electro-deposition. However, these methods include disadvantages, like low selectivity, limited removal efficiency, high-energy requirements, and consumption of large amounts of chemicals (Shuhong *et al.* 2014). Compared with the conventional technologies mentioned, adsorption seems to be one of the most efficient methods for the removal of different heavy metal ions from industrial effluents because of its wide range of applications and simple operation (Thilagavathy and Santhi 2014).

Adsorption processes that utilize commercially available activated carbon (AC) are generally expensive because of the high production cost of AC. For this reason, a lot of research effort is being devoted to finding new precursors from inexpensive sources, like agricultural waste, which will yield AC that has a superior adsorbing capacity compared to commercially available AC (Krishnan *et al.* 2011; Saka 2012). Various modifications on the surface of lignocellulosic-based AC are also being explored to further improve their pore structure and properties.

The chemical activation of biomass involves the impregnation of the precursor with a chemical, followed by a heating treatment. Compared with other chemical activating agents such as sulfuric acid, potassium hydroxide, and zinc chloride, the use of phosphoric acid has been reported to promote the development of a mesoporous surface on lignocellulosic precursors. A mesoporous surface is desirable for the adsorption of pollutants such as heavy metals (Li *et al.* 2010). It has also been reported to activate the lignocellulosic precursor at a lower activation temperature (about 450 °C) than potassium hydroxide (above 700 °C), with less toxic residues compared to zinc chloride (Sun *et al.* 2016).

The utilization of response surface method (RSM) in optimizing independent variables is particularly advantageous when the parameters being studied, including their levels and responses, are not yet fully understood. A standard RSM design of experiment called a central composite design (CCD) is preferred for generating a quadratic response surface. A CCD also helps to analyze the interaction between the factors and to determine the optimum parameters, with a minimal number of experiments (Alslaibi *et al.* 2013).

This study focused on the preparation, optimization, and characterization of phosphoric acid activated mahogany fruit husk (MFH) using RSM following a CCD. Batch adsorption experiments were performed to investigate the effect of activation parameters, such as the percent concentration of phosphoric acid (H_3PO_4%), heating temperature, and holding time, on the removal of Cr^{6+} from an aqueous solution. The adsorption equilibrium data was analyzed using the Langmuir and Freundlich isotherm models, while the adsorption kinetic studies were performed and fitted using pseudo-first and pseudo-second-order kinetic models.

EXPERIMENTAL

Preparation of Aqueous Solution

A stock solution of hexavalent chromium with a concentration of 1000 mg/L was prepared by dissolving a sufficient amount of potassium dichromate ($K_2Cr_2O_7$) in distilled water. The standards and solutions for the adsorption experiments were obtained by diluting the stock solution to the desired concentrations. For the pH adjustments, 0.1 M HCl and 0.1 M NaOH were used. All chemicals utilized in this work were of analytical reagent (AR) grade.

Design of Experiment

The independent variables utilized in this study were H_3PO_4% (*A*), heating temperature (*B*), and holding time (*C*). Each independent variable was varied over three levels between *-1* and *+1* at specific ranges. Table 1 shows the variables and their corresponding levels.

Table 1. Independent Variables and their Coded Levels for the Central Composite Design (CCD)

Factors	Code	Units	Coded variable levels		
			-1	*0*	*+1*
H_3PO_4	A	% (v/v)	30	40	50
Heating temperature	B	°C	400	600	800
Holding time	C	Min	30	60	90

For the central composite design (CCD) with three factors, the number of tests required included the standard 2*k* points with the origin located at the center, 2*k* points fixed axially at a distance, and replicate tests at the center, where *k* is the number of factors. The axial points were assigned so that they allowed for readability, which was to ensure that the variance of the model prediction was constant at all points equidistant from the design center (Sahu *et al.* 2009). Hence, the total number of experiments for this study was 20 (from 2*k* + 2*k* + 8), where the number of factors (*k*) was 3. The performance of the process was evaluated by analyzing the percent hexavalent chromium removal efficiency of the derived AC.

The optimization and response surface modelling of the chromium (VI) removal efficiency of the phosphoric acid activated carbon from MFH were done using the Design-Expert® (Stat-Ease Inc., Minneapolis, MN, USA) software. An analysis of variance (ANOVA) was carried out to test for the validity of the generated model. The goodness-of-fit of the obtained responses with the model was established by using the correlation coefficient (R^2). The model's Fisher variation ratio (*F*-value), probability value (Prob. > *F*), and adequate precision (AP) were also evaluated to test for its significance and adequacy.

Preparation of Activated Carbon

The MFH was locally obtained from Batangas City, Philippines. It was rinsed three times with distilled water to remove soluble impurities and then dried in an oven at 105 °C for 24 h. The dried samples were ground and sieved to a particle size of approximately 800 µm. The carbonization was carried out for 1 h by loading a dried precursor into a stainless steel vertical tube reactor under purified nitrogen flow. The activation process of the MFH was performed according to the run order listed in Table 2 for the CCD. The char was chemically activated using H_3PO_4 as the impregnating agent. The carbonized MFHs were soaked in varying percent concentrations of phosphoric acid (30%, 40%, and 50% v/v) with an impregnation ratio of 1:2 (w/w of char and H_3PO_4 solution) for 2 h at 80 °C. Afterwards, the samples were filtered and oven dried for 24 h at 105 °C. The thermal treatment of the impregnated chars was carried out using a muffle furnace at different temperature levels (400, 600, and 800 °C) and holding times (30, 60, and 90 min). The derived AC was cooled to room temperature, and washed with hot deionized water and 0.1 M HCl until the filtrate reached a pH of 6 to 7. The MFHAC samples were oven dried for 24 h at 105 °C and stored in air-tight containers.

Characterization of Optimized MFHAC

A volumetric adsorption analyzer (Quantachrome, Boynton Beach, FL, USA) was used to study the surface properties of the optimized MFHAC. The surface area, total pore volume, and average pore diameter of the optimized MFHAC prepared under optimum conditions were obtained through the analysis of the N_2 adsorption isotherms at -196 °C. The BET surface area was measured from the adsorption isotherm using the Brunauer–Emmett–Teller (BET) equation. The total pore volume was estimated to be the liquid volume of nitrogen at a relative pressure of 0.99. The surface morphology of the optimized MFHAC and the detection of the adsorbed chromium onto the MFHAC were investigated using a JSM-5310 (JEOL Ltd., Tokyo, Japan) scanning electron microscope equipped with an energy-dispersive X-ray spectrometer (EDS). The surface functional groups of the AC were determined using a Nicolet 6700 (Thermo Nicolet Co., Madison, WI, USA) Fourier-transform infrared (FTIR) spectrophotometer.

Batch Adsorption Studies

The batch adsorption process was performed for the hexavalent chromium adsorption onto the derived AC. Following the CCD of the experiment, 20 adsorption tests were conducted. Each flask contained 50 mL of 50 mg/L Cr^{6+} aqueous solution. The prepared AC samples (0.10 g) were added to the individual flasks, which were then agitated with an isothermal shaker set at 30 °C and 200 rpm until the equilibrium time of 1 h was reached. After agitation, the samples were filtered immediately using Whatman #1 filter paper (Sigma-Adrich Pte. Ltd, Nucleos, Singapore) to separate the adsorbent from the solution. During filtration, the samples were divided into two parts. The first part was used to saturate the filter paper to avoid the effects of adsorption onto the filter paper and the filtrate was disregarded. The residual Cr^{6+} concentrations in the filtrate from the second portions were measured using a GENESYS 5 (Spectronic Co., Waltman, MA, USA) double beam UV-Visible spectrophotometer at 540 nm upon compleximetric reaction with 1,5-diphenylcarbazide at a pH of 2.0. The adsorbed Cr^{6+} concentrations were obtained from the difference between the initial and final concentrations in the solution, while the percentage removal at equilibrium was calculated based on the following equation,

$$Cr^{6+}\ removal\ (\%) = [(C_o - C_e) / C_o] \times 100 \tag{1}$$

where C_o and C_e are the liquid-phase concentrations of the initial state and at equilibrium (mg/L), respectively. The amount of Cr^{6+} adsorbed per unit mass of the derived AC at equilibrium time, q_e (mg/g), was calculated using Eq. 2,

$$q_e = [(C_o - C_e)V] / m \quad (2)$$

where q_e (mg/g) is the amount of Cr^{6+} adsorbed per unit weight of adsorbent, C_o and C_e (mg/L) are the liquid-phase concentrations of adsorbate at the initial and equilibrium conditions, respectively, V (L) is the volume of the solution, and m (g) is the mass of the derived AC used.

Adsorption Isotherms

In this study, the Langmuir and Freundlich models were employed to describe the adsorption mechanism of Cr^{6+} onto the surface of the optimized MFHAC.

Langmuir model

The Langmuir isotherm model is based on the assumption of monolayer adsorption onto a surface with the equivalent and identical number of localized sites (Langmuir 1916). The maximum adsorption is achieved when the surface is covered by a monolayer of the adsorbate. The linear form of the Langmuir isotherm is expressed by the following equation,

$$(1 / q_e) = (1 / Q_b C_e) + (1 / Q) \quad (3)$$

where C_e (mg/L) is the equilibrium liquid-phase concentration of Cr^{6+}, q_e (mg/g) is the equilibrium uptake capacity, Q (mg/g) is the Langmuir constant related to the adsorption capacity, and b (L/mg) is the Langmuir constant related to the sorption energy, which quantitatively describes the interaction between the adsorbent and the adsorbate.

Freundlich model

The Freundlich model is valid for multilayer adsorption onto a heterogeneous surface with a varying distribution of active sites (Freundlich 1906). This isotherm model does not describe any adsorbate saturation. Instead, infinite surface coverage is mathematically predicted. The linear form of the Freundlich isotherm is expressed by the following equation,

$$\log q_e = \log K + (1 / n) \log C_e \quad (4)$$

where q_e (mg/g) is the amount of Cr^{6+} adsorbed at equilibrium, C_e (mg/L) is the adsorbate concentration, K_f (mg/g)(L/mg)$^{1/n}$ is the Freundlich constant related to the adsorption capacity, and $1/n$ is the Freundlich constant related to sorption intensity of the sorbent.

Adsorption Kinetics

The adsorption kinetics studies were done in order to describe the rate of Cr^{6+} uptake onto the optimized MFHAC, and provided major insight into the adsorption mechanism and the possible rate-controlling processes, mass transfer, and chemical reaction. The controlling mechanism of the adsorption process was investigated by fitting the experimental data with pseudo-first-order and pseudo-second-order kinetic models.

Pseudo-first-order model

The adsorption of liquid-solid systems based on the solid capacity follows a pseudo-first-order model (Lagergren 1898). Generally, the pseudo-first-order kinetic model is only applicable for the initial stage of the adsorption process. The linear form of the pseudo-first-order rate equation is illustrated by the following equation,

$$\log (q_e - q_t)^t = \log (q_e) - (k_1 t / 2.303) \tag{5}$$

where k_1 (1/min) is the pseudo-first-order adsorption rate constant, and q_e and q_t are the amount of adsorbed Cr^{6+} in mg/g at the equilibrium time and at time t (min), respectively.

Pseudo-second-order model

The pseudo-second-order model predicts the adsorption mechanism over a range of different points in time during the adsorption process. The pseudo-second-order model equation is given as,

$$(t / q_t) = (1 / k_2 q_e^2) + (t / q_e) \tag{6}$$

where k_2 (g/mg·min) is the equilibrium rate constant of the pseudo-second-order model.

RESULTS AND DISCUSSION

A total of 20 experiments were conducted to develop a response surface model (RSM) for the Cr^{6+} removal efficiency of the AC prepared from MFH at varying H_3PO_4%, heating temperatures, and holding times. The experimental factors used in this study and their responses are listed in Table 2. The results from the experiment revealed Cr^{6+} removal efficiencies that varied from 27.1% to 91.8%.

Table 2. Experimental Factors and Responses

Std. No.	Run No.	Point Type	Factors			Cr^{6+} Removal (%)
			A: H_3PO_4 (% v/v)	B: Temp. (°C)	C: Time (min)	
1	7	Fact	30	400	30	39.61
2	16	Fact	50	400	30	38.31
3	18	Fact	30	800	30	27.08
4	13	Fact	50	800	30	31.17
5	15	Fact	30	400	90	62.34
6	5	Fact	50	400	90	48.03
7	12	Fact	30	800	90	45.45
8	2	Fact	50	800	90	30.32
9	4	Axial	30	600	60	65.58
10	9	Axial	50	600	60	55.45
11	3	Axial	40	400	60	91.84
12	17	Axial	40	800	60	85.58
13	8	Axial	40	600	30	64.42
14	11	Axial	40	600	90	77.39
15	19	Center	40	600	60	86.51
16	20	Center	40	600	60	89.83
17	10	Center	40	600	60	87.57
18	1	Center	40	600	60	87.42
19	14	Center	40	600	60	88.69
20	6	Center	40	600	60	88.20

Statistical Analysis

An analysis of variance (ANOVA) was performed to evaluate the acceptability of the model. The results of the second-order response surface model fitting for Cr^{6+} removal are given in Table 3. The quality of the model developed was evaluated based on the correlation coefficient (R^2) and standard deviation. The model was significant at the 5% confidence level.

A model is considered to demonstrate a good fit if the coefficient of determination reaches a value of 0.80 and above (Bashir *et al.* 2010). The closer R^2 is to 1, the more accurate and reliable the response will be predicted by the model. A high R^2 value of 0.9954 was obtained in the present study, which indicated that only 0.46% of the total variation was unexplained by the generated model.

The ANOVA results for the quadratic response surface model for Cr^{6+} removal had an F-value of 370.9363 and a corresponding probability greater than F that was less than 0.05, which indicated that the model was significant. For the model terms, probability factor (Prob. > F) values less than 0.05 are considered significant. In this work, the model terms A, B, C, AC, BC, A^2, and C^2 were significant, while AB and B^2 were insignificant terms. To improve the model's efficiency, the insignificant model terms were excluded from the study.

Table 3. Analysis of Variance of the Quadratic Model for the Chromium (VI) Removal Efficiency of the Derived MFHAC

Source of data	Sum of Squares	Degrees of freedom	Mean Square	F - Value	Prob. > F	Comment
Model	10347.34	7	1478.191	370.9363	< 0.0001	significant
A-H_3PO_4	135.2768	1	135.2768	33.94628	< 0.0001	significant
B-Temp	366.3881	1	366.3881	91.94118	< 0.0001	significant
C-Time	396.1444	1	396.1444	99.40820	< 0.0001	significant
AC	129.8466	1	129.8466	32.58362	< 0.0001	significant
BC	27.86311	1	27.86311	6.991951	0.0214	significant
A^2	2719.695	1	2719.695	682.4784	< 0.0001	significant
C^2	1126.576	1	1126.576	282.7021	< 0.0001	significant
Residual	47.82032	12	3.985027			
Lack of Fit	41.22199	7	5.888856	4.462381	0.0594	not sig.
Pure Error	6.598333	5	1.319667			
Std. Dev. = 2.00 CV = 3.09 AP = 51.326				R^2 = 0.9954 Adjusted R^2 = 0.9927 Predicted R^2 = 0.9826		

The adequate precision (AP) measures the ratio between the signal and noise, and determines whether the predicted model can be used to move along the design space (Bashir *et al.* 2010). AP values higher than 4 are desirable. A high AP ratio of 51.3 was obtained, and suggested that the model can navigate in the space defined by the CCD utilized in this work. The obtained coefficient of variance (CV) value of 2.47% was below 10%, which meant that the model for Cr^{6+} removal gave reproducible results. Based on the statistical data obtained, the model presented in this work was efficient and able to predict the Cr^{6+} removal within the established set of parameters. The final regression model with respect to the variables used is shown by the following equation,

$$Cr^{6+}\ removal\ (\%) = 88.50 - 3.68A - 6.05B + 6.29C - 4.03AC - 1.87BC - 29.15A^2 - 18.76C^2 \quad (7)$$

where A is the H_3PO_4% (30% to 50% v/v), B is the heating temperature (400 °C to 800 °C), and C is the holding time (30 min to 90 min).

The activation process of MFH using phosphoric acid and heat treatment in a furnace was optimized with the Design-Expert software. The simultaneous evaluation of different combinations of the factors used (H_3PO_4%, heating temperature, and holding time) at various levels and their responses was performed to determine the optimum activation conditions for MFH that will yield the highest Cr^{6+} removal efficiency. The optimum conditions and the corresponding predicted and actual Cr^{6+} removal efficiencies are presented in Table 4. The experiment was performed in triplicate to validate the Cr^{6+} removal efficiency of the optimized MFHAC. As shown in Table 4, the obtained experimental 92.29% Cr^{6+} removal from a 50 mg/L Cr^{6+} solution was in close agreement with the predicted removal efficiency of 94.3022%. The relative percent error between the predicted and obtained experimental values was 2.13%, which validated the reliability of the generated predictive model and the goodness-of-fit with the experimental results.

Table 4. Experimental Confirmation of the Predicted Cr^{6+} Removal Efficiency of the MFHAC Prepared Under the Optimum Conditions

Factor			Predicted Cr^{6+} removal (%)	Actual Cr^{6+} removal* (%)	Relative Error (%)
H_3PO_4 (% v/v)	Temp. (°C)	Time (min)			
39.55	428.72	70.58	94.3022	92.29	2.134
**Average of triplicate analysis*					

To further illustrate the effect of the relationships among the variables of H_3PO_4%, heating temperature, and holding time on the responses predicted by the model, three dimensional (3D) surface response plots were generated. In the plots shown in Fig. 1, one variable was kept constant at the optimum value, while the two remaining parameters were varied within their experimental ranges. Figure 1a shows the 3D response surface of the combined effects of the H_3PO_4% and heating temperature, while the holding time was kept at the optimum value of 70.58 min. The maximum Cr^{6+} removal was observed when the char was chemically impregnated with about 40% H_3PO_4, followed by a heat treatment at around 430 °C. This suggested that pore development was improved when relatively high amounts of H_3PO_4 was introduced into the char followed by a thermal treatment at temperatures near 430 °C, which led to the formation of improved active sites. Beyond the optimum heating temperature, the pores of the AC may have started to break down, which explained the decreased removal efficiency.

Figure 1b illustrates the 3D response plot of the combined effects of the holding time and H_3PO_4% at a constant heating temperature of 428.72 °C. The maximum Cr^{6+} removal efficiency was observed when both parameters were at approximately the middle values of their respective ranges. The H_3PO_4 promoted the development of pores by initially occupying cavities in the char. When thermally treated, the H_3PO_4 molecules swelled and eventually volatilized. The porous structure was produced from the voids left by the H_3PO_4 molecules (Girgis and El-Hendawy 2002). At the optimum holding time of 70.58 min, most of the H_3PO_4 would have already volatilized, which left only the developed pores. The continued heating beyond the optimum holding time may have caused the newly developed pores to break, and resulted in a reduced Cr^{6+} removal efficacy.

Figure 1c shows the 3D response surface of the combined effects of the heating temperature and holding time, while the H_3PO_4% was held constant at 39.55%. The contour plot demonstrated an improvement in the Cr^{6+} removal at an increased holding time of up to 70 min. However, the increased Cr^{6+} removal was seen only up to a heating temperature of about 430 °C. This may have been explained by the fact that as the heating temperature increased above the optimum level, the active sites started to disintegrate, which resulted in a decrease in the Cr^{6+} removal. Holding times above 70 min may have caused the pores to rupture, which explained the reduction in the Cr^{6+} adsorption.

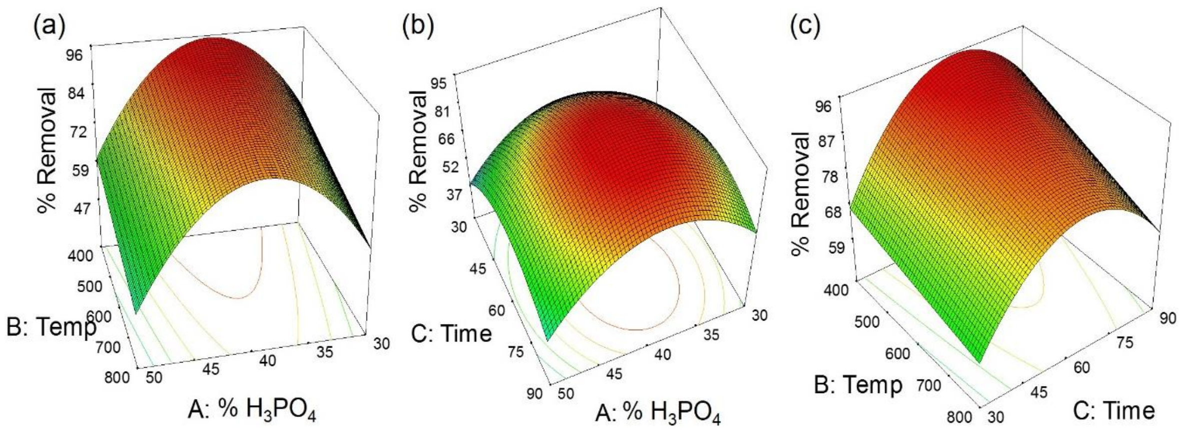

Fig. 1. 3D response plots of the Cr^{6+} removal efficiencies of the optimized MFHAC with respect to the effects of (a) heating temperature and H_3PO_4%, (b) holding time and H_3PO_4%, and (c) heating temperature and holding time

Surface Characteristics of the Optimized MFHAC

Figure 2 shows the SEM images of the optimized MFHAC before and after Cr^{6+} adsorption. It can be seen in Fig. 2a that the MFHAC derived under the optimum conditions developed a porosity that consisted of macropores. The presence of the deep macropores and micropores, along with varied cavities on the surface of the MFHAC suggested a well-developed pore structure. The developed pore structures provided a higher probability for Cr^{6+} entrapment and adsorption onto the surface of the MFHAC.

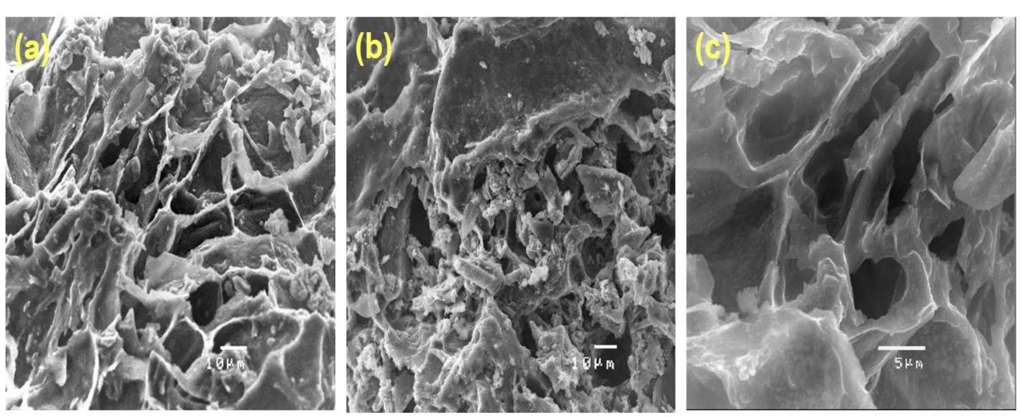

Fig. 2. SEM images of (a) MFHAC before adsorption (1000x), and Cr^{6+} loaded MFHAC at (b) 1000x and (c) 3500x magnification

Figures 2b and c show the SEM morphology of MFHAC loaded with Cr^{6+}. As can be seen in Fig. 2c, a new layer was formed on the surface of the MFHAC.

The EDX spectra of the optimized MFHAC, before and after Cr^{6+} adsorption, are illustrated in Figure 3. Based on the spectrum shown in Figure 3a, the derived MFHAC consisted mainly of C, N, O, and P, along with other elements such as Na, S, and K. The new peaks at around 0.45 and 5.40 keV were detected in the surface of the Cr^{6+} loaded MFHAC (Fig. 3b). This confirmed the adsorption of Cr on the surface of the optimized MFHAC. A decrease in the intensity of the P peak was also seen in spectrum of the Cr^{6+} loaded MFHAC (Fig. 3b). The same results were observed in the works of Cheng *et al.* (2016) and Maneechakr and Karnjanakom (2017).

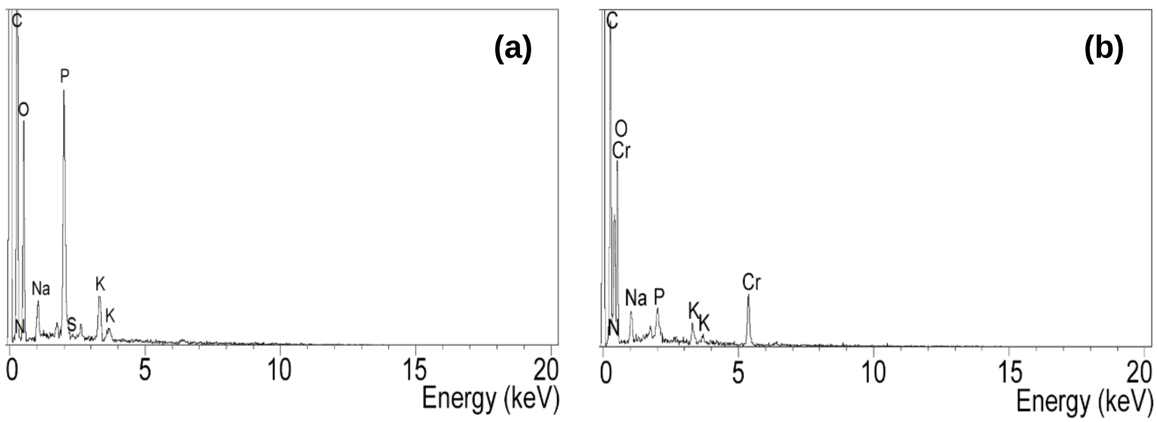

Fig. 3. EDX spectra of (a) MFHAC before adsorption and (b) Cr^{6+} loaded MFHAC

To further understand the mechanisms on how the Cr^{6+} ions get adsorbed on the surface of the MFHAC, FTIR studies were employed on the optimized MFHAC, before and after Cr^{6+} adsorption. The FTIR spectra for the optimized MFHAC and the Cr^{6+} loaded MFHAC are presented in Fig. 4. The intensity at around 3414 cm^{-1} indicated the presence of H from hydroxyl groups (Cheng *et al.* 2006). There were also narrow bands present at around 2918 and 2849 cm^{-1} that related to C–H of alkyl structures (Günzler and Bock 1990; Zhang *et al.* 2010), which were due to methyl (CH_3) and methylene (CH_2) asymmetric stretching. The absorption energy near 2284 cm^{-1} is characteristic of the possible presence of nitriles or isocyanates. An absorbance band was also visible at 1702 cm^{-1} for C=O stretching (Chiang *et al.* 2000). The intensity at 1615 cm^{-1} indicates the presence of aromatic and olefinic C=C and C=O of bonded conjugated ketones, aldehydes, quinines, and aromatic groups (Wang *et al.* 2009). The peak observed at 1511 cm^{-1} indicated the presence of N-H stretching from amines and amide groups, and nitro compounds (Simha *et al.* 2016). The band at 1081 cm^{-1} in the MFHAC suggests the presence of stretching vibration of C–O functional groups, including alcohols, ethers, acids, and esters (Sharma *et al.* 2004). The presence of hydroxyl groups, carbonyl groups, and ethers is evidence that the structure of the MFHAC contained lignocellulose. The functional groups mentioned above have been reported to exhibit a high affinity toward Cr^{6+} ions (Rai *et al.* 2016). This was confirmed in the FTIR spectrum of MFHAC loaded with Cr^{6+} illustrated in Fig. 4. The observed decrease in transmittance intensity and shifts in peak locations at different frequencies suggested the interactions between the Cr^{6+} ions and the functional groups present in the surface of the MFHAC. Similar observations were also seen in the studies of Cheng *et al.* (2016) and Rai *et al.* (2016).

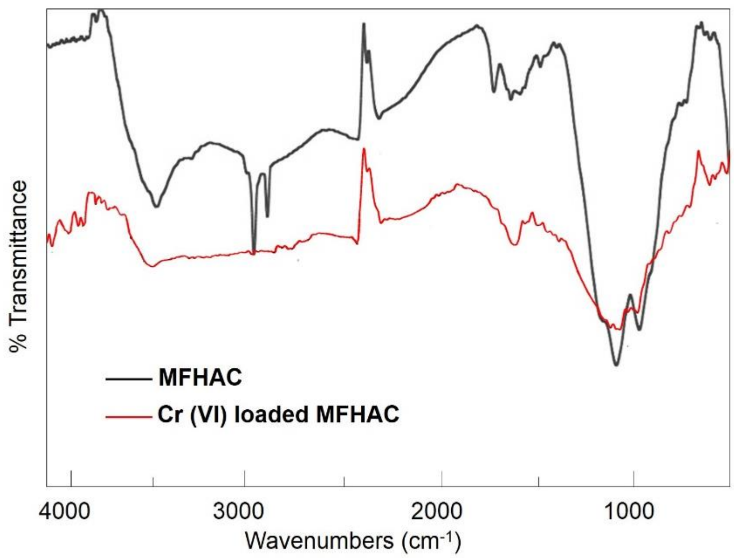

Fig. 4. FTIR spectra of (a) MFHAC before adsorption and (b) Cr^{6+} loaded MFHAC

The MFHAC prepared under the optimum conditions had a BET surface area (S_{BET}) of 1128 m^2/g with a total pore volume (V_T) of 0.832 cm^3/g and a mean pore diameter (D) of 3.41 nm. The developed porous carbon structure of the MFHAC may have been attributed to the employment of phosphoric acid as the activating agent that accompanied heating at around 430 °C. Chemical impregnating agents, like H_3PO_4, work by dehydrating the char. This results in the lowering of the activation temperature necessary during chemical activation, and thereby, further promoting a well-developed porous structure in the resulting AC (Girgis and El-Hendawy 2002).

Adsorption Isotherms

The equilibrium isotherm parameters and correlation coefficients obtained from linear fitting with the Langmuir and Freundlich isotherm models are shown in Table 6.

Table 6. Langmuir and Freundlich Isotherm Parameters for the Adsorption of Chromium (VI) onto the MFHAC

Langmuir Isotherm Model				Freundlich Isotherm Model		
Q (mg/g)	K_L	R_L	R^2	K_f	*1/n*	R^2
46.71	0.5736	0.4346	0.9935	28.94	0.1530	0.9785

The equilibrium data from the adsorption isotherm studies of the Cr^{6+} ions onto the MFHAC were fitted and linearized using the Langmuir and Freundlich isotherm models. The linear form of the Langmuir model (Fig. 5a) was obtained by plotting C_e against C_e/q_e, while the linear form of the Freundlich isotherm (Fig. 5b) was achieved from the plot of ln q_e against ln C_e. The determined correlation coefficient (R^2) values from the line fitting of the equilibrium data using the Langmuir and Freundlich isotherm models were 0.9935 and 0.9785, respectively. The lower R^2 of 0.9785 of the linear Freundlich isotherm plot suggested less precise fit between the Freundlich model and the equilibrium data. In contrast, the high R^2 of the linear Langmuir isotherm plot revealed good agreement between the Langmuir parameters and the experimental results of the equilibrium studies.

This revealed that the adsorption of Cr^{6+} occurred *via* monolayer adsorption of the Cr^{6+} ions onto the internal and external surface of the MFHAC. The favorability of the equilibrium data with the Langmuir model was further supported by the computed separation factor (R_L) value of 0.4346. An R_L that is between 0 and 1 corresponds to an adsorption that is favorable toward the Langmuir model.

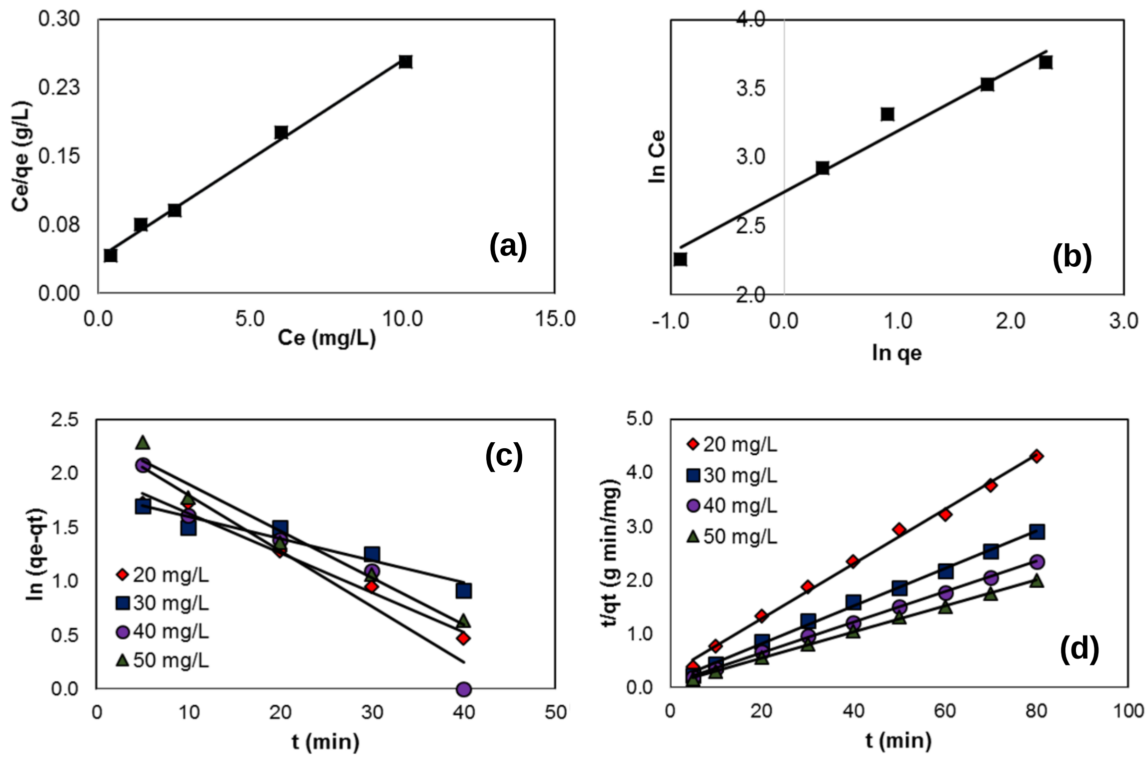

Fig 5. (a) Langmuir and (b) Freundlich isotherm plots for the adsorption of Cr^{6+} onto MFHAC; (c) Pseudo-first-order and (d) Pseudo-second-order kinetic model plots of Cr^{6+} onto MFHAC for different initial concentrations

Adsorption Kinetics

Table 7 presents the kinetic parameters for the pseudo-first-order and pseudo-second-order kinetic models for the adsorption of Cr^{6+} onto the MFHAC prepared under optimum conditions.

Table 7. Kinetic Parameters for the Adsorption of Chromium (VI) onto the MFHAC at Different Initial Concentration

C_o (mg/L)	q_e (exp) (mg/g)	Pseudo-first-order			Pseudo-second-order		
		K_1 (min^{-1})	q_e (cal) (mg/g)	R^2	K_2 (g/mg min)	q_e (cal) (mg/g)	R^2
20	18.54	0.0437	10.02	0.8472	0.0096	19.71	0.9958
30	27.42	0.0391	13.43	0.7811	0.0097	28.64	0.9966
40	34.11	0.0506	15.42	0.8611	0.0107	35.12	0.9992
50	46.71	0.0460	24.57	0.8501	0.0094	44.88	0.9972

The maximum adsorption capacity (q_e) of 46.71 mg/g was experimentally determined at a constant temperature of 30 °C. As shown in Table 7, low correlation coefficient (R^2) values were obtained for the pseudo-first-order model at different Cr^{6+} initial concentrations, which indicated there was poor agreement of the kinetics data with the pseudo-first-order model of the adsorption of Cr^{6+} onto the adsorbent. In contrast, high R^2 values (Table 7) were obtained for the linear plots of (t/q_t) *versus* t for the pseudo-second-order equation for different Cr^{6+} initial concentrations. The high R^2 values obtained suggested that the adsorption of Cr^{6+} onto the surface of MFHAC followed pseudo-second-order kinetics, suggesting that the adsorption of the Cr^{6+} onto the MFHAC may have taken place *via* diffusion of the Cr^{6+} ions across the external boundary layer and in the internal micropores of the AC, which was consistent with the findings reported in literature (Hubbe *et al.* 2012a,b). It was also observed that there was good agreement between the experimental and calculated maximum adsorption capacity (q_e) values, which further confirmed the goodness-of-fit of the kinetics data with the model. The obtained maximum Cr^{6+} adsorption capacity (46.7 mg/g) of the optimized MFHAC was comparable to the reported adsorption capacities of the other adsorbents listed in Table 8. The considerably high Cr^{6+} adsorption capacity obtained in this work indicated the efficacy of the MFHAC for removing Cr^{6+} in aqueous solution.

Table 8. Comparison of Cr (VI) Adsorption Capacities of Different Adsorbents

Adsorbent	Cr^{6+} Adsorption Capacity (mg/g)	Reference
Mango seed kernel	8.85	(Rai *et al.* 2016)
Oak bark	4.93	(Mohan *et al.* 2011)
Oak wood	7.51	
Tire waste	12.45	(Nieto-Márquez *et al.* 2017)
Tamarind wood	28.02	(Acharya *et al.* 2009)
Almond shells	20.0	(Demirbas *et al.* 2004)
Neem Bark	19.60	(Dakiky *et al.* 2002)
Bael fruit shell	43.54	(Gottipati and Mishra 2016)
Mahogany fruit husk	46.71	This study
Apricot stones	108.08	(Özdemir *et al.* 2011)

CONCLUSIONS

1. The activation of MFH was successfully optimized using RSM through chemical impregnation with 39.6% H_3PO_4 (v/v), followed by a heat treatment at 428.7 °C for 70.6 min. The optimized MFHAC exhibited a high removal efficiency of 92.3% from a 50 mg/L Cr^{6+} aqueous solution at 30 °C.
2. A quadratic response surface model equation that can be used for the prediction of Cr^{6+} removal efficiencies of the MFHAC prepared at varying H_3PO_4%, heating temperatures, and holding times was successfully developed.
3. The MFHAC prepared under the optimum conditions had a well-developed porous surface structure with a high surface area (S_{BET}) of 1128 m^2/g. It also contained functional groups that exhibited interactions with the Cr^{6+} ions during adsorption.
4. The adsorption equilibrium data demonstrated the best fit with the Langmuir isotherm model, which indicated a monolayer adsorption process. The adsorption kinetic data for different Cr^{6+} initial concentrations were best explained by the pseudo-second-order

kinetic model. The obtained maximum Cr^{6+} adsorption capacity (46.7 mg/g) of the optimized MFHAC was comparable with the adsorption capacities of other reported adsorbents.

ACKNOWLEDGMENTS

The authors are grateful to Batangas State University, Philippines for providing the facilities to conduct this study, and to Ms. Nora L. Talain of the Bureau of Soils – Region IV, Philippines, and Dr. Christina A. Binag of RCNAS, University of Santo Tomas, Philippines for their technical support.

REFERENCES CITED

Acharya, J., Sahu, J. N., Sahoo, B. K., Mohanty, C. R., and Meikap, B. C. (2009). "Removal of chromium(VI) from wastewater by activated carbon developed from tamarind wood activated with zinc chloride," *Chem. Eng. J.* 150(1), 25-39. DOI: 10.1016/j.cej.2008.11.035

Al-Othman, Z. A., Naushad, M., and Inamuddin. (2011). "Organic–inorganic type composite cation exchanger poly-o-toluidine Zr(IV) tungstate: Preparation, physicochemical characterization and its analytical application in separation of heavy metals," *Chem. Eng. J.* 172(1), 369-375. DOI: 10.1016/j.cej.2011.06.018

Baral, A., and Engelken, R. D. (2002). "Chromium-based regulations and greening in metal finishing industries in the USA," *Environ. Sci. Policy* 5(2), 121-133. DOI: 10.1016/S1462-9011(02)00028-X

Bashir, M. K. J., Aziz, H. A., Yusoff, M. S., and Adlan, M. N. (2010). "Application of response surface methodology (RSM) for optimization of ammoniacal nitrogen removal from semi-aerobic landfill leachate using ion exchange resin," *Desalination* 254(1-3), 154-161. DOI: 10.1016/j.desal.2009.12.002

Brauer, S. L., and Wetterhahn, K. E. (1991). "Chromium(VI) forms a thiolate complex with glutathione," *J. Am. Chem. Soc.* 113(8), 3001-3007. DOI: 10.1021/ja00008a031

Chen, Z., Cheng, Y., Zhou, F., and Li, S. (2016). "Removal of mixed contaminants crystal violet and heavy metal ions by immobilized stains as the functional biomaterial," *RSC Adv.* DOI: 10.1039/C6RA13337A

Cheng, C. -H., Lehmann, J., Thies, J. E., Burton, S. D., and Engelhard, M. H. (2006). "Oxidation of black carbon by biotic and abiotic processes," *Org. Geochem.* 37(11), 1477-1488. DOI: 10.1016/j.orggeochem.2006.06.022

Chiang, H. -L., Tsai, J. -H., Tsai, C. -L., and Hsu, Y. -C. (2000). "Adsorption characteristics of alkaline activated carbon exemplified by water vapor, H_2S, and CH_3SH gas," *Separ. Sci. Technol.* 35(6), 903-918. DOI: 10.1081/SS-100100200

Dakiky, M., Khamis, M., Manassra, A., and Mer'eb, M. (2002). "Selective adsorption of chromium(VI) in industrial wastewater using low-cost abundantly available adsorbents," *Adv. Environ. Res.* 6(4), 533-540. DOI: 10.1016/S1093-0191(01)00079-X

Demirbas, D., Kobya, M., Senturk, E., and Ozkan, T. (2004). "Adsorption kinetics for the removal of chromium (VI) from aqueous solutions on the activated carbons prepared from agricultural wastes," *Water SA* 30, 533. DOI: 10.4314/wsa.v30i4.5106

Freundlich, H. M. F. (1906). "Over the adsorption in solution," *J. Phys. Chem-US* 57, 385-471.

Girgis, B. S., and El-Hendawy, A. -N. A. (2002). "Porosity development in activated carbons obtained from date pits under chemical activation with phosphoric acid," *Micropor. Mesopor. Mat.* 52(2), 105-117. DOI: 10.1016/S1387-1811(01)00481-4
Gładysz-Płaska, A., Majdan, M., Pikus, S., and Sternik, D. (2012). "Simultaneous adsorption of chromium(VI) and phenol on natural red clay modified by HDTMA," *Chem. Eng. J.* 179, 140-150. DOI: 10.1016/j.cej.2011.10.071
Gottipati, R., and Mishra, S. (2016). "Preparation of microporous activated carbon from Aegle Marmelos fruit shell and its application in removal of chromium(VI) from aqueous phase," *Journal of Industrial and Engineering Chemistry, 36,* 355-363. DOI: 10.1016/j.jiec.2016.03.005
Günzler, H., and Bock, H. (1990). *IR-Spektroskopie* [*IR-Spectroscopy*], Verlag Chemie, Weinheim, Germany.
Hubbe, M. A., Hasan, S. H., and Ducoste, J. J. (2012). "Cellulosic substrates for removal of pollutants from aqueous systems: A review. 1. Metals," *BioResources* 6(2), 2161-2287. DOI: 10.15376/biores.7.2.2592-2687
Hubbe M. A., Beck, K. R., O'Neal, W. G., and Sharma, Y. C. (2012). "Cellulosic substrates for removal of pollutants from aqueous systems: A review. 2. Dyes," *BioResources* 7(2), 2592-2687. DOI: 10.15376/biores.7.2.2592-2687
Jayakumar, R., Rajasimman, M., and Karthikeyan, C. (2014). "Sorption of hexavalent chromium from aqueous solution using marine green algae *Halimeda gracilis*: Optimization, equilibrium, kinetic, thermodynamic and desorption studies," *J. Environ. Chem. Eng.* 2(3), 1261-1274. DOI: 10.1016/j.jece.2014.05.007
Krishnan, K. A., Sreejalekshmi, K. G., and Baiju, R. S. (2011). "Nickel(II) adsorption onto biomass based activated carbon obtained from sugarcane bagasse pith," *Bioresour. Technol.* 102(22), 10239-10247. DOI: 10.1016/j.biortech.2011.08.069
Kushwaha, S., Sreedhar, B., and Sudhakar, P. P. (2012). "A spectroscopic study for understanding the speciation of Cr on palm shell based adsorbents and their application for the remediation of chrome plating effluents," *Bioresour. Technol.* 116, 15-23. DOI: 10.1016/j.biortech.2012.04.009
Lagergren, S. (1898). "About the theory of so-called adsorption of soluble substances," *Kungliga Svenska Vetenskapsakademiens Handlingar* 24(4), 1-39.
Langmuir, I. (1916). "The constitution and fundamental properties of solids and liquids," *J. Am. Chem. Soc.* 38(11), 2221-2295. DOI: 10.1021/ja02268a022
Li, K., Zheng, Z., and Li, Y. (2010). "Characterization and lead adsorption properties of activated carbons prepared from cotton stalk by one-step H_3PO_4 activation," *J. Hazard. Mater.* 181(1–3), 440-447. DOI:
Maneechakr, P. and Karnjanakom, S. (2017). "Adsorption behaviour of Fe(II) and Cr(VI) on activated carbon: Surface chemistry, isotherm, kinetic and thermodynamic studies," *The Journal of Chemical Thermodynamics* 106, 104-112.
Mohan, D., Rajput, S., Singh, V. K., Steele, P. H., and Pittman Jr, C. U. (2011). "Modeling and evaluation of chromium remediation from water using low cost bio-char, a green adsorbent," *J. Hazard. Mater.* 188(1–3), 319-333. DOI: 10.1016/j.jhazmat.2011.01.127
Nieto-Márquez, A., Pinedo-Flores, A., Picasso, G., Atanes, E., and Sun Kou, R. (2017). "Selective adsorption of Pb^{2+}, Cr^{3+} and Cd^{2+} mixtures on activated carbons prepared from waste tires," *J. Environ. Chem. Eng,* 5(1), 1060-1067. DOI: 10.1016/j.jece.2017.01.034

Özdemir, E., Duranoğlu, D., Beker, Ü., and Avcı, A. Ö. (2011). "Process optimization for Cr(VI) adsorption onto activated carbons by experimental design," *Chem. Eng. J.,* 172(1), 207-218. DOI: 10.1016/j.cej.2011.05.091

Rai, M. K., Shahi, G., Meena, V., Meena, R., Chakraborty, S., Singh, R. S., and Rai, B. N. (2016). "Removal of hexavalent chromium Cr (VI) using activated carbon prepared from mango kernel activated with H_3PO_4," *Resource-Efficient Technologies*, 2, Supplement 1, S63-S70. DOI: 10.1016/j.reffit.2016.11.011

Sahu, J. N., Acharya, J., and Meikap, B. C. (2009). "Response surface modeling and optimization of chromium(VI) removal from aqueous solution using tamarind wood activated carbon in batch process," *J. Hazard. Mater.* 172(2–3), 818-825. DOI: 10.1016/j.jhazmat.2009.07.075

Saka, C. (2012). "BET, TG–DTG, FT-IR, SEM, iodine number analysis and preparation of activated carbon from acorn shell by chemical activation with $ZnCl_2$," *J. Anal. and Appl. Pyrol.* 95, 21-24. DOI: 10.1016/j.jaap.2011.12.020

Setshedi, K. Z., Bhaumik, M., Songwane, S., Onyango, M. S., and Maity, A. (2013). "Exfoliated polypyrrole-organically modified montmorillonite clay nanocomposite as a potential adsorbent for Cr(VI) removal," *Chem. Eng. J.* 222, 186-197. DOI: 10.1016/j.cej.2013.02.061

Sharma, R. K., Wooten, J. B., Baliga, V. L., Lin, X., Chan, W. G., and Hajaligol, M. R. (2004). "Characterization of chars from pyrolysis of lignin," *Fuel* 83(11–12), 1469-1482. DOI: 10.1016/j.fuel.2003.11.015

Shuhong, Y., Meiping, Z., Hong, Y., Han, W., Shan, X., Yan, L., and Jihui, W. (2014). "Biosorption of Cu^{2+}, Pb^{2+} and Cr^{6+} by a novel exopolysaccharide from *Arthrobacter* ps-5," *Carbohyd. Polym.* 101, 50-56. DOI: 10.1016/j.carbpol.2013.09.021

Simha, P., Mathew, M., and Ganesapillai, M. (2016). "Empirical modeling of drying kinetics and microwave assisted extraction of bioactive compounds from Adathoda vasica and Cymbopogon citrates," *Alexand. Eng. J*. 55(1), 141–150.

Sun, Y., Li, H., Li, G., Gao, B., Yue, Q., and Li, X. (2016). "Characterization and ciprofloxacin adsorption properties of activated carbons prepared from biomass wastes by H_3PO_4 activation," *Bioresour. Technol.* DOI: 10.1016/j.biortech.2016.03.047

Thilagavathy, P., and Santhi, T. (2014). "Kinetics, isotherms and equilibrium study of Co(II) adsorption from single and binary aqueous solutions by *Acacia nilotica* leaf carbon," *Chinese J. Chem. Eng.* 22(11–12), 1193-1198. DOI: 10.1016/j.cjche.2014.08.006

Wang, S., Wang, K., Liu, Q., Gu, Y., Luo, Z., Cen, K., and Fransson, T. (2009). "Comparison of the pyrolysis behavior of lignins from different tree species," *Biotechnol. Adv.* 27(5), 562-567. DOI: 10.1016/j.biotechadv.2009.04.010

World Health Organization. (2011). *Guidelines for Drinking-Water Quality (4th ed.)*, World Health Organization Press, Geneva, Switzerland.

Zhang, H., Tang, Y., Cai, D., Liu, X., Wang, X., and Huang, Q. (2010). "Hexavalent chromium removal from aqueous solution by algal bloom residue derived activated carbon: Equilibrium and kinetic studies," *J. Hazard. Mater.* 181, 801-808.

Article submitted: November 4, 2016; Peer review completed: January 20, 2017; Revised version received: February 23, 2017; Accepted: February 24, 2017; Published: March 2, 2017.
DOI: 10.15376/biores.12.2.3001-3016